Antibody Therapeutics, 2025, 8(4), 350–363
https://doi.org/10.1093/abt/tbaf025
Advance access publication date 4 November 2025
Research Article

Assessing the therapeutic potential of a panel of novel VCAM-1 antibodies using microfluidic and three-dimensional *in vitro* models of vascular inflammation

Jessica R. Pickett[1,2], Lucia F. Zacchi[3,4], Binura Perera[1], Yuao Wu[1], Hang Thu Ta[1,2]

[1]School of Environment and Science, Griffith University, 170 Kessels Road, Nathan, Queensland 4111, Australia
[2]Queensland Quantum and Advanced Technologies Research Institute, Griffith University, 170 Kessels Road, Nathan, Queensland 4111, Australia
[3]School of Chemistry and Molecular Biosciences, The University of Queensland, 280-284 Sir Fred Schonell Drive, St Lucia, Queensland 4072, Australia
[4]Australian Institute for Bioengineering and Nanotechnology, The University of Queensland, 280-284 Sir Fred Schonell Drive, St Lucia, Queensland 4072, Australia
*Corresponding author. School of Environment and Science, Griffith University, 170 Kessels Road, Nathan, Queensland, Australia. E-mail: h.ta@griffith.edu.au

Abstract

Objective: Antibodies against vascular cell adhesion molecule (VCAM)-1 represent an attractive strategy for atherosclerosis and cardiovascular disease management due to their ability to selectively block leukocyte-endothelial interactions involved in inflammatory cell recruitment. Herein, seven novel anti-VCAM-1 monoclonal antibodies (mAbs) generated from phage display biopanning were tested using a series of *in vitro* models of cell recruitment to determine their potential utility for treating atherosclerosis.
Methods and Results: We assessed the inhibitory effects of the test antibodies on cell adhesion and transmigration using a series of *in vitro* assays that incorporated three-dimensional microfluidics and collagen hydrogel models. In summary, each of our mAb candidates were found to reduce RAW264.7 monocyte adhesion to activated SVEC4–10 endothelial monolayers under static conditions. Subsequently, the three most effective candidates from this assay—2E2, 3C12, and 3H4—were shown to inhibit monocyte adhesion to endothelial microvessels under flow conditions and monocyte transmigration into endothelialized gel matrices under static conditions.
Conclusion: These results indicate that our novel anti-VCAM-1 mAbs can effectively inhibit monocyte adhesion and transmigration *in vitro*, supporting the therapeutic rationale of VCAM-1 immunoblockade for the targeted treatment of atherosclerosis.

Graphical Abstract

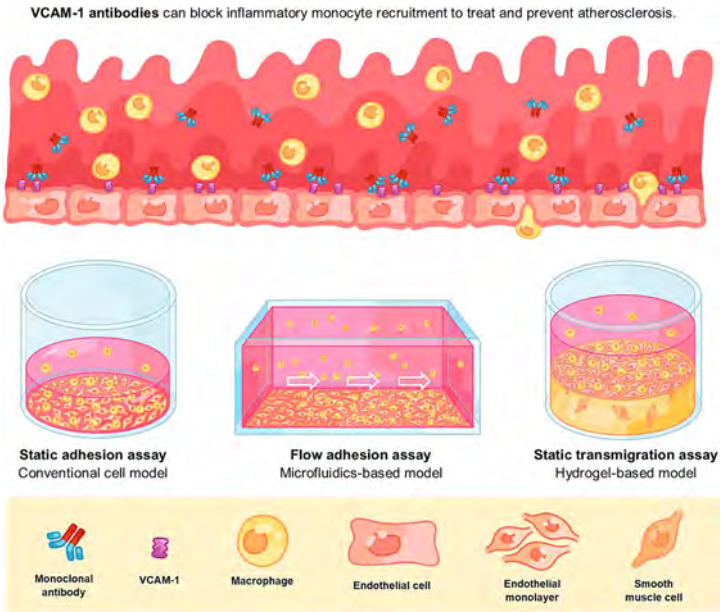

Received: May 26, 2025. **Revised:** September 19, 2025. **Accepted:** October 12, 2025

Statement of Significance
This study provides valuable insights for antibody drug discovery technologies and pre-clinical models of cardiovascular diseases.

Keywords: vascular cell adhesion molecule; VCAM-1; antibody therapy; atherosclerosis; monocyte; endothelial cell

Introduction

Atherosclerosis is a degenerative vascular condition that involves the progressive build-up of lipid-laden plaque (also known as 'atheroma') in inflamed arteries, eventually resulting in narrowed vessels that obstruct normal blood flow [1]. One of the most dangerous aspects of the disease is its insidious nature, often completely evading clinical detection until it has already culminated in life-threatening complications such as myocardial infarction or ischaemic stroke [2]. Traditionally, the treatment and prevention of atherosclerosis-related cardiovascular diseases (CVDs) has been focused primarily on managing classical cardiac risk factors, such as hypertension and hypercholesterolaemia [3]. However, despite the efficacy of existing pharmacological interventions in controlling these established health risks, CVD remains the leading cause of mortality globally [4]. More recently, the scientific understanding of atherosclerosis has evolved to recognize the role of the innate immune response– particularly of dysregulated monocyte recruitment –in the development and progression of atherosclerotic lesions [5]. As such, there has been a notable shift in research attention towards novel therapies that focus on directly countering the inflammatory pathogenesis of atherosclerotic lesion formation [6].

Therapeutic antibodies that selectively target cell adhesion and recruitment at atheromatous lesions and lesion-predisposed regions present an attractive avenue for anti-atherosclerotic drug development [7]. Cell adhesion molecules (CAMs) facilitate the attachment and transmigration of monocytes across the vessel wall into the subendothelial space before they transform into the lipid-engorged foam cells that constitute the atherosclerotic plaque [1]. Naturally, several CAM-inhibiting agents, including high-affinity antibodies, have been investigated as novel therapeutics for atherosclerosis [7]. In particular, antibodies against vascular cell adhesion molecule (VCAM)-1 have attracted significant research attention for their capacity to selectively bind to inflamed regions of the vascular endothelium during atherosclerosis while avoiding adjacent, non-inflamed tissues [8]. However, the therapeutic potential of anti-VCAM-1 antibodies for treating atherosclerotic lesions has been somewhat overshadowed by their usefulness as targeting ligands in vectorized drug delivery systems [9]. Currently, a study by Park *et al.* [10] assessing the effects of novel anti-VCAM-1 antibodies in hypercholesterolemic mouse models remains the most comprehensive investigation of the therapeutic potential of VCAM-1 antibodies for treating atherosclerosis.

Current advancements in antibody discovery technologies have allowed researchers to generate a vast arsenal of novel anti-VCAM-1 antibodies that may also be suitable as future drug candidates [8, 11]. Though the most extensively studied anti-VCAM-1 antibody candidates tend to target the first and second domains of the protein, researchers have more recently begun to investigate the effects of targeting adjacent and alternative domains on receptor binding activity and signalling function [10–12]. Therefore, in optimizing the production pipeline of new antibodies for therapeutic use, improving disease modelling platforms for pre-clinical drug testing has become increasingly necessary. The limitations of conventional cell-based models to simulate the physiological conditions of the vascular environment have fuelled the demand for improved *in vitro* technologies that can serve as better platforms for disease modelling and drug testing. In particular, microfluidic devices incorporating pulsatile flow and three-dimensional (3D) cell culture models that simulate the layered vascular architecture are the predominant approaches for improving *in vitro* modelling of atherosclerosis [13]. Implementing these techniques allows researchers to better replicate biological processes involved in atherosclerotic lesion formation, such as inflammatory cell recruitment, to reliably examine the therapeutic mechanisms and efficacy of novel drug candidates.

This study employs a series of *in vitro* assays modelling pathological monocyte recruitment during vascular inflammation to preliminarily evaluate the therapeutic potential of seven novel anti-VCAM-1 monoclonal antibodies (mAbs) as possible drug candidates for atherosclerosis. In our recent work (Perera *et al.* [11]), these antibody candidates—1A9, 2D3, 2D8, 2E2, 2E6, 3C12, and 3H4—identified by phage display biopanning and in scFv format, were shown to reduce monocyte adhesion to activated endothelial monolayers *in vitro* (with the exception of clone 3C12, which was not tested). However, monocyte recruitment involves several molecular processes outside of leukocyte-endothelial attachment and, thus, further experimentation is required to reliably predict the effects of our test antibodies in the human vascular environment. To achieve this, we employed a microfluidics-based microvessel model to measure antibody inhibition of cell adhesion under human physiological flow conditions and a 3D intimal model to assess cell transmigration under static conditions using murine cell lines. This research holds considerable implications for the medical application of VCAM-1 mAbs for the targeted treatment of atherosclerotic lesions. Moreover, this study also validates the utility of microfluidics- and hydrogel-based atherosclerosis models for the *in vitro* testing of novel therapeutics targeting cell recruitment.

Materials and method

The full description of materials and methods is provided in Supporting Information.

Development and selection of anti-VCAM-1 mAbs

Before the commencement of this project, a panel of anti-VCAM-1 mAbs (1A9, 2D3, 2D8, 2E2, 2E6, 3C12, and 3H4) with binding affinity to mouse VCAM-1 was generated. Phage display biopanning was used to screen a human naïve single-chain variable fragment (scFv) library for clones specifically binding mouse VCAM-1. The scFvs were reformatted into full-length, mouse immunoglobulin G $(IgG)_{2a}$ mAbs and expressed in mammalian cells following standard protocols [11, 14]. The known binding specificities of the scFvs for each of the seven IgG domains of VCAM-1 are listed in Table 1 (with further information in Supplementary Fig. S1).

Table 1. List of the Ig-like domain binding specificities of the seven novel anti-VCAM-1 antibody candidates and the positive control anti-VCAM-1 antibody used in this study

Antibody name	RRID	Domain specificity for VCAM-1 protein
429 (MVCAM)	AB_467419	Domain 1
1A9	–	Domain 3
2D3	–	Domain 2
2D8	–	Domain 3
2E2	–	Domain 3
2E6	–	Domain 5
3C12	–	Domain 1
3H4	–	Domain 2

Other antibodies

Other antibodies used in this study are as follows. Rat anti-mouse anti-VCAM-1 (CD106) 429 mAb (Thermo Fisher Scientific #14–1061-82, RRID: AB_467419), rat anti-mouse VE-cadherin (CD144, Alexa Fluor® 488) BV13 mAb (Thermo Fisher Scientific #53–1441-80, RRID: AB_1210528), and mouse IgG_{2a} isotype control (Thermo Fisher Scientific #02–6502, RRID: AB_2532951) were purchased from Thermo Fisher Scientific.

Static monocyte adhesion assay on the microplate

The static monocyte-endothelial cell adhesion assay was adapted from Park *et al.* [10] SVEC cells were seeded in 96-well plates and cultured in DMEM for 24 h, then stimulated with 100 ng/ml LPS for another 24 h. Cells were pre-treated with 20 μg/ml anti-VCAM-1 antibodies (including positive control, isotype control, and test clones) for 1 h. Meanwhile, RAW monocytes were labelled with 50 ng/ml $DiOC_6$, washed, and added to the wells (1.0×10^4 cells/well), followed by a 10 min incubation at 37°C in the dark. Wells were then washed to remove unbound cells and fixed with 4% PFA.

Fluorescence spectrophotometry and microscopy of static binding assay

Monocyte adhesion was quantified using two methods: fluorescence plate reader analysis and fluorescence microscopy (full details are provided in the Supporting Information). Cumulative fluorescence from $DiOC_6$-labelled monocytes was measured and normalized to control wells. Microscopy images were analyzed using Fiji software to count adherent cells, providing an average cell density per unit area (mm^2) [15].

Microfluidics chip fabrication

Microfluidics chips were fabricated according to standard photolithography and polydimethylsiloxane (PDMS) soft lithography techniques [16]. The PDMS mixture was cast onto a silicon mould, cured, and bonded to glass slides via oxygen plasma treatment. The final device featured a single rectangular microchannel with defined inlet and outlet ports, suitable for cell culture and flow-based assays. For this study, the design of the microfluidic device consisted of a single rectangular microchannel chamber (255 μm wide and 100 μm high) with circular inlet and outlet ports (100 μm in diameter).

Microvessel formation in the microfluidics device

Endothelial cells were seeded within the microfluidic devices using a protocol previously reported by Akther *et al.* [17] Briefly, endothelial cells were seeded into sterilized, collagen-coated microfluidic devices [18] to promote adhesion. A high-density SVEC cell suspension was injected, followed by incubation under oscillatory flow and standard culture conditions to form a uniform 3D endothelial microvessel. The device was connected to a peristaltic pump and maintained under physiological flow rates, starting low (12 μl/min) and increasing to arterial shear conditions (31 μl/min) over 24 h to support vessel formation. This flow rate was calculated to equate to typical arterial shear rate (1000 s^{-1}) based on the dimensions of the microchannel and Newton's Law of Viscosity [19]. All treatments were subsequently perfused at this flow rate.

Flow-based monocyte adhesion assay on the microfluidic chip

After forming a confluent endothelial monolayer, microvessels were stimulated with 1 μg/ml LPS for 8 h, followed by a 2 h pre-treatment with 20 μg/ml anti-VCAM-1 antibodies. Fluorescently labelled RAW monocytes were then perfused through the microchannel to assess monocyte rolling and adhesion under flow using fluorescence microscopy. Adhesion was quantified by counting Hoechst-labelled cells per mm^2 from three randomly selected fields within the microchannel at 20× magnification (0.5 mm^2/field) using Fiji software.

Formation of cell-hydrogel constructs for 3D cell culture

Cell-hydrogel constructs were prepared using collagen I and MOVAS smooth muscle cells to model the subendothelial environment. The collagen and smooth muscle cell components of the resultant hydrogel matrices served to model the extracellular microenvironment of the vascular subendothelial space [20]. After gelation in 96-well plates, constructs were endothelialized with SVEC cells and cultured for 5 days to form a confluent monolayer [21]. Endothelial barrier integrity was confirmed via VE-cadherin immunostaining and assessed by brightfield and fluorescence microscopy.

Monocyte transmigration assay under static, non-flow conditions

Once endothelial monolayers reached confluency, constructs were stimulated with 100 ng/ml LPS for 24 h, followed by a 1 h pre-treatment with 20 μg/ml anti-VCAM-1 antibodies. RAW monocytes were then added and incubated for 1 h to allow adhesion. Non-adherent cells were collected and counted using a haemocytometer. Constructs were then replenished with fresh media and incubated for 24 h to allow cell migration before further analysis.

Visual assessment of monocyte transmigration by Giemsa stain microscopy

To qualitatively assess monocyte transmigration, cell-hydrogel constructs were stained with Giemsa, which selectively labels leukocytes [22, 23]. After fixation, standard staining and washing steps were followed. Gels were then placed on coverslips for brightfield microscopy, and monocytes were counted on both the endothelial surface and within the hydrogel matrix from randomly selected fields within the microplate wells at 20× magnification (0.5 mm^2/field).

Quantitative measurement of transmigration by Giemsa smear

To quantify monocyte adhesion and transmigration, an adapted Giemsa smear method was used [24]. Non-transmigrated

monocytes were detached from the hydrogel surface using trypsin, collected, and stained for counting *via* Giemsa smear. Transmigrated cells were isolated by enzymatic digestion of the gel with collagenase, followed by centrifugation and staining using the same smear protocol. Cells were visualized and counted under brightfield microscopy to assess antibody efficacy.

Statistical analysis

Data are presented as mean ± standard deviation, with statistical significance indicated by $^{*}P < .05$, $^{**}P < .01$, $^{***}P < .005$, $^{**}P < .001$. Group comparisons were performed using one-way ANOVA with Tukey's post-hoc testing. All analyses were conducted using GraphPad Prism 10. The total number of experimental replicates (N), which includes both independent experiments and technical replicates, are indicated in the figure legends for each experiment.

Results

Novel VCAM-1 antibodies decreased monocyte attachment to inflamed endothelial monolayers under static conditions

Prior to this study, Perera *et al.* [11] generated a panel of novel anti-VCAM-1 antibodies by phage display biopanning of a human naïve scFv library. In summary, a pool of seven novel mAb candidates—1A9, 2D3, 2D8, 2E2, 2E6, 3C12, and 3H4—was selected based on their binding to seven-domain, murine VCAM-1. As part of the study, the scFv antibody fragments (with the exception of 3C12, which was not included) were tested for their capacities to inhibit monocyte-endothelial adhesion, which is a critical process in vascular inflammation. All the tested candidates were able to significantly reduce monocyte attachment to activated endothelial cells, except for 2E6 ($P = .056$) [11]. These scFvs were reformatted into full-length, mouse IgG_{2a} mAbs [11] and used in this study.

To validate and compare the immunoblockade effects of the selected full-length mAbs on VCAM-1-mediated cell-to-cell interactions, we performed conventional cell adhesion assays quantifying monocyte attachment to endothelial monolayers *in vitro*. As a proof-of-concept, a precursory cell adhesion assay was performed to verify the effects of inflammatory LPS stimulation and VCAM-1 immunoblockade on monocyte-endothelial interactions. Briefly, confluent endothelial monolayers were pre-treated or not with LPS, and LPS-treated samples were also treated with culture media alone (no antibody), anti-VCAM-1429 mAb, or a non-VCAM-1-binding negative control for 1 h and then incubated with suspensions of fluorescent monocytes for 10 min before rinsing with DPBS. As summarized in (Fig. 1e), this assay demonstrated that inflammatory stimulation by LPS treatment (Fig. 1b) significantly increased ($P < .001$) monocyte attachment compared to the non-treated control group (Fig. 1a). These observations are corroborated by previous studies demonstrating the stimulatory effects of LPS induction on monocyte-endothelial interactions [25, 26]. Moreover, preincubation of cell monolayers with positive control anti-VCAM-1429 mAb (Fig. 1c) after LPS stimulation was shown to significantly reduce ($P < .001$) the mean level of monocyte adhesion to a level that was comparable to that observed with the non-stimulated endothelia (Fig. 1a). This ability of the 429 mAb to inhibit adhesion of RAW264.7 monocytes to SVEC4–10 monolayers was similar to that of two novel anti-VCAM-1 mAbs (H6 and 7H) tested previously by Park *et al.* [10] to inhibit the adhesion of U937 monocytes to tumour necrosis factor-α–stimulated HUVEC monolayers. Further, the negative control (mouse IgG_{2a} isotype control, a non-VCAM-1 antibody binder) was unable to reduce monocyte adhesion to SVEC4–10 cells upon LPS stimulation (Fig. 1d), indicating that the impact of the 429 antibody treatment on adhesion is due to VCAM-1 blockade.

The static adhesion assay was then employed to assess the potential therapeutic effects of the anti-VCAM-1 mAb panel generated from phage display biopanning by Perera *et al.* [11] Using the commercial anti-VCAM-1429 control mAb from the preliminary assay as a reference, we evaluated the inhibitory activity of each of the seven candidates on adhesive monocyte-endothelial interactions. For quantitative analysis, the signal intensity of each well was measured by fluorescent spectrophotometry (Fig. 2m), and the number of adherent cells per unit area (Fig. 2n) was calculated from fluorescent microscopy images (Fig. 2a–l). As expected based on the scFv results [11], several of the mAb candidates effectively reduced ($P < .05$) monocyte adhesion compared to the LPS-stimulated control group (Fig. 2b) (Supplementary Table S1) [11]. Based on the spectrophotometry data (Fig. 2m), three mAbs from the candidate panel demonstrated levels of efficacy (Supplementary Table S2) that were more statistically similar to the commercial anti-VCAM-1 antibody: 2E2 ($P > .9999$), 3C12 ($P = .6409$), and 3H4 ($P = .1604$). Notably, pre-incubating the inflamed cell monolayers with a mouse IgG_{2a} isotype negative control antibody (Fig. 2d) did not significantly reduce ($P > .05$) monocyte adhesion compared to the LPS-treated group, supporting the conclusion that the blockade in adhesion is a VCAM-1-mediated effect. Although we cannot rule out an impact of Fc receptors binding the anti-VCAM-1 antibodies on our study, our data clearly shows that our mouse anti-mVCAM-1 antibody can significantly adhesion of murine monocytes to murine endothelial cells. A similar result was obtained by Park *et al.* [10] with their fully human H6 and 7H anti-hVCAM-1 antibodies on HUVECs and U937 cells.

VCAM-1 antibodies decreased leukocyte rolling and adhesion on endothelial microvessels under flow conditions

Following the static adhesion assay, the three most effective antibodies– 2E2, 3C12, and 3H4 –were tested on a microfluidics-based vascular platform that observed leukocyte rolling and arrest under physiological flow conditions. This model consisted of a 3D endothelial microvessel enclosed within a PDMS microfluidic chip template and subjected to constant peristaltic flow. The channel design and dimensions of the microfluidic chip (Fig. 3a, b) had been determined prior to this study in previous experiments by Akther *et al.* [19] modelling the vascular environment during inflammatory disease. While the SVEC4–10 and RAW264.7 cell lines employed in this model are murine in origin, the peristaltic flow rate (31 μl/min) was intentionally chosen to mimic the physiological arterial shear rate (1000 s^{-1}) observed in the human vasculature [19]. Brightfield microscopy images (Fig. 4c, d) confirmed the successful formation of a confluent endothelial monolayer on the microchannel surface that could be maintained under constant exposure to flow for several days. Using brightfield and fluorescent microscopy techniques, the microfluidic model allows for the real-time visualization and quantification of adhesive cell-to-cell interactions between rolling monocytes and endothelial microvessels under physiological flow conditions. Therefore, this device could be utilized as an *in vitro* platform for modelling and predicting the therapeutic efficacy of our anti-VCAM-1 mAb candidates on monocyte-endothelial interactions in the human vascular microenvironment.

This microfluidic model of vascular inflammation was then utilized to determine whether the three selected test antibodies could inhibit leukocyte rolling and adhesion under physiological

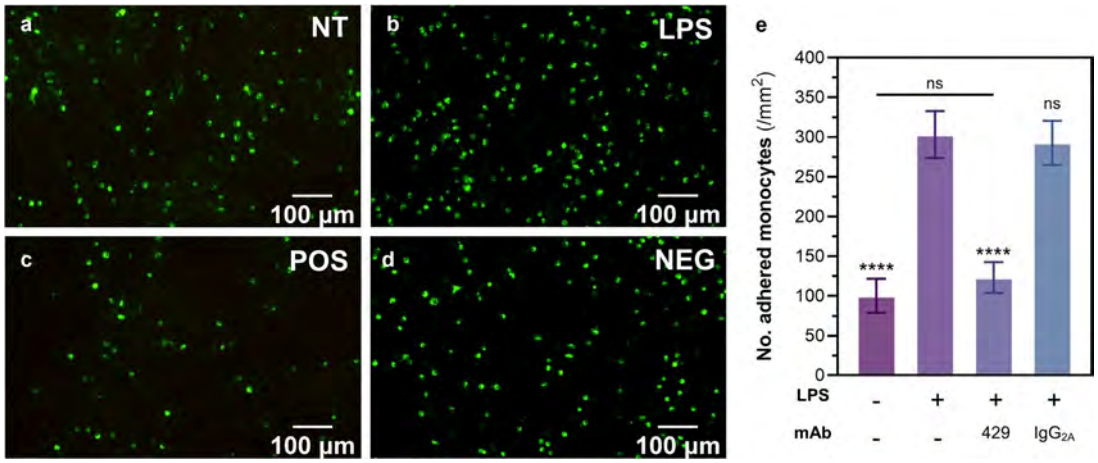

Figure 1. Preliminary adhesion assay assessing the effects of LPS stimulation and VCAM-1 antibody blockade on adhesive monocyte-endothelial interactions. (a-d) Representative fluorescent microscopy (20×) images of labelled RAW264.7 monocytes attached to SVEC4-10 endothelial monolayers pre-treated with (a) non-supplemented cell culture media, (b) LPS, (c) LPS followed by anti-VCAM-1 429 mAb treatment, and (d) LPS stimulation followed by a non-VCAM-1 binder treatment as negative control (mouse IgG2a isotype control antibody). (e) Graphical comparison of cell adhesion with LPS stimulation and anti-VCAM-1 antibody blockade. Cell adhesion was quantified by counting labelled cells in 3 random fields of view observed at 20× magnification, then calculating the number of adhered monocytes per mm2. The graph shows the mean +/- SD of 4 independent experiments with 2 sample replicates each (total N = 8) analyzed by ANOVA and post-hoc Tukey testing. Asterisk labels indicate statistical significance of the non-treated control and mAb treatment groups compared to the LPS-stimulated group unless otherwise specified. ns $p > 0.05$, *$p < 0.05$, **$p < 0.01$, ***$p < 0.001$, ****$p < 0.0001$.

flow conditions. In brief, endothelial microvessels were pre-incubated with LPS for inflammatory stimulation, administered with test antibody, and then perfused with fluorescently labelled monocytes for the flow adhesion assay. Cell attachment was visualized by fluorescent microscopy images (Fig. 4a–f) taken at 10-min intervals after initiating monocyte perfusion and then subsequently quantified from automatic cell counting. Figure 4g demonstrates that LPS stimulation (Fig. 4b) significantly increased ($P < .05$) monocyte adhesion to the endothelial microvessel at all time points compared to the non-treated group (Fig. 4a). Furthermore, VCAM-1 immunoblockade treatment with the commercial anti-VCAM-1429 mAb (Fig. 4c) was able to significantly reduce ($P < .01$) monocyte adhesion to stimulated endothelia, much like in the static adhesion assay (Fig. 4).

For both the non-treated and LPS-stimulated control groups, cell attachment increased consistently between each of the 10-min time points (Fig. 4g). Like in the static adhesion assay, the amount of cell attachment under flow was significantly higher ($P < .05$) with LPS treatment at all the measured time points compared to the non-treated group (Fig. 4a, b, g, h). As expected, all the antibody-treated groups were able to maintain stable levels of minimal cell adhesion after the initial amount of monocyte attachment recorded at the 10-min time point. Of the novel mAb candidates, 2E2 was the most effective in blocking monocyte-endothelial interactions under flow, decreasing the number of adhered monocytes at 30-min by 85.5% compared to the LPS-stimulated group (Fig. 4b, d, g, h). To note, unlike in the static adhesion assay (Fig. 2), the antibody-treated groups decreased the number of adhered monocytes under flow to a level significantly below ($P < .05$) that observed for the non-treated control group. This observation suggests that our microfluidics-based assay model involves background levels of adhesion that are not attributed to inflammatory stimulation by LPS. Endothelial expression of VCAM-1 without chemical stimulation has been reported in the literature, in which shear stress upregulates surface VCAM-1 and increases monocyte adhesion *via* inducible cell signalling pathways [27, 28], which could explain our results. Our findings are consistent with previous studies demonstrating the capacity of anti-VCAM-1 mAbs to decrease monocyte rolling and adhesion on atherosclerotic carotid arteries *ex vivo* [29, 30].

VCAM-1 antibodies reduced leukocyte transmigration into 3D cell-hydrogel constructs under static conditions

To generate a comprehensive picture of monocyte recruitment during atherosclerotic lesion formation, it is necessary to evaluate the effects of drug candidates not only on cell adhesion, but also on cell migration. For this reason, we tested the three selected novel anti-VCAM-1 mAbs—2E2, 3C12, and 3H4—on a hydrogel-based cell model used previously to model monocyte recruitment and foam cell formation *in vitro* [21]. The cell-hydrogel construct model employed for our purpose comprised an endothelial/smooth muscle cell co-culture involving an SVEC4–10 monolayer seeded atop a MOVAS-laden collagen gel matrix. To confirm the successful formation of a confluent endothelial monolayer atop the hydrogel surface, we monitored daily cell proliferation using brightfield microscopy (Fig. 5a–f). VE-cadherin immunostaining visually confirmed endothelial contact integrity, with the homogenous distribution of fluorescence indicating adherens junctions had been established between endothelial cells at confluency (Fig. 5g, h). Therefore, this hydrogel-based model could be used to evaluate the effects of our novel mAb candidates on endothelial barrier function and vascular permeability by quantifying monocyte transmigration into the gel matrix.

Using this hydrogel-based 3D cell culture model, we investigated the ability of our novel anti-VCAM-1 mAb candidates to inhibit monocyte-endothelial adhesion and transendothelial migration *in vitro*. To do this, LPS-stimulated cell-hydrogel constructs were pre-treated with 20 μg/ml anti-VCAM-1 mAbs for 1 h and then incubated with monocyte cell suspensions for 1 h before replenishing the media and incubating for a further 24 h. As demonstrated in Fig. 6, we were able to visually differentiate

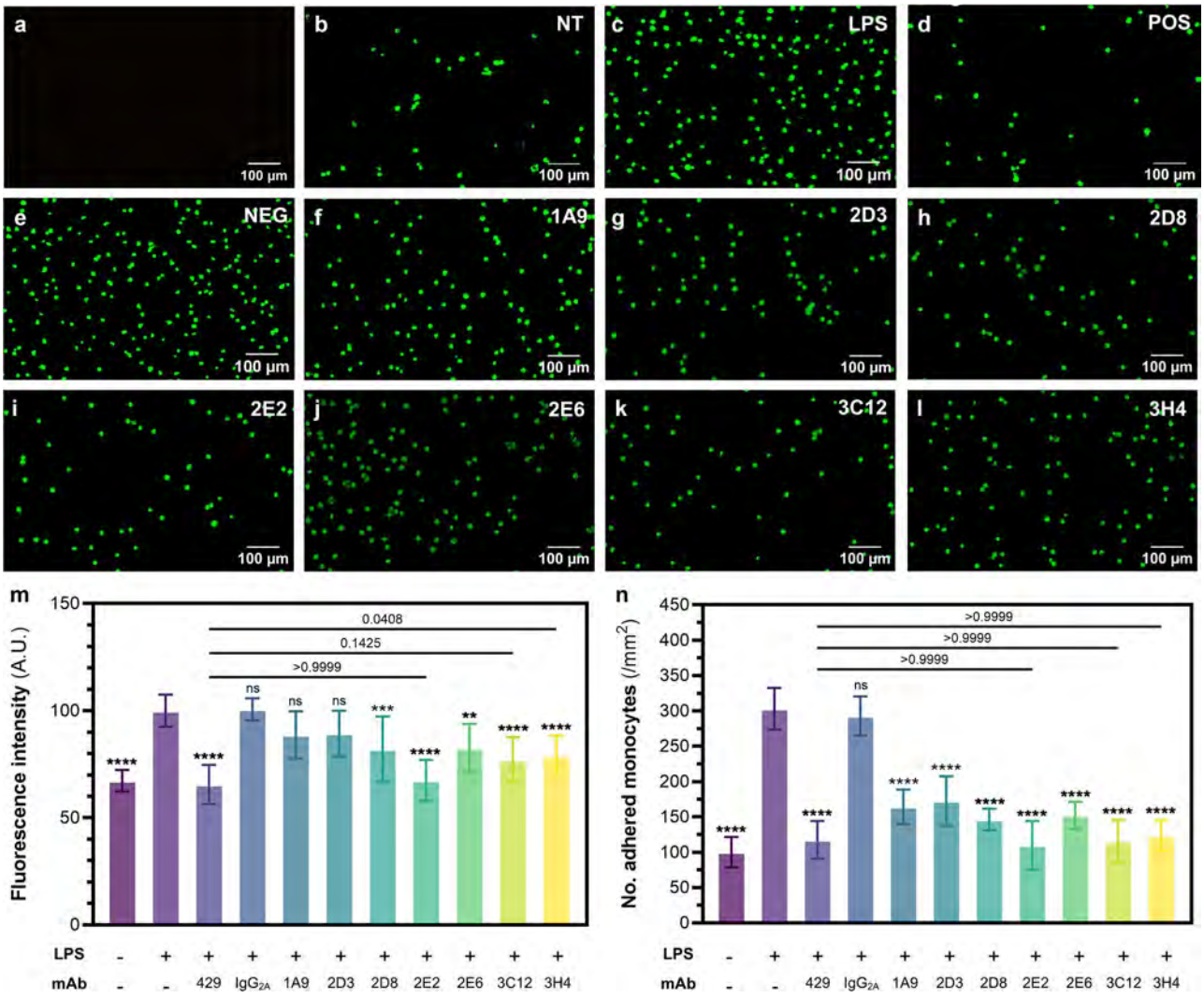

Figure 2. Competitive adhesion assay assessing the potential therapeutic capabilities of a panel of novel anti-VCAM-1 mAb candidates to inhibit monocyte-endothelial interactions under static conditions. (a-k) Representative fluorescent microscopy (20×) images of labelled RAW264.7 monocytes attached to SVEC4-10 endothelial monolayers. This includes a (a) blank control of endothelial monolayers receiving no fluorescent monocyte treatment. For samples that were subjected to monocyte treatment, cell monolayers were pre-incubated with (b) non-supplemented cell culture media, with (c) LPS, or LPS stimulation followed by treatment with (d) commercial anti-VCAM-1 429 mAb (positive control), (e) negative mouse IgG2a isotype mAb, (f) 1A9 mAb, (g) 2D3 mAb, (h) 2D8 mAb, (i) 2E2 mAb, (j) 2E6 mAb, (k) 3C12 mAb, or (l) 3H4 mAb. Monocyte adhesion was then quantified and compared based on the (m) mean fluorescence intensity of sample wells measured by spectrophotometry and the (n) number of adhered monocytes per mm2 calculated from cell counts of 3 random fields of view observed at 20× magnification (0.5 mm2). Graph M shows the mean +/- SD of 4 independent experiments with 3 sample replicates each (total N = 12) and Graph N shows the mean of 2 independent experiments with 3 sample replicates each and 2 independent experiments with 2 sample replicates each (N = 10) analyzed by ANOVA and post-hoc Tukey testing. Asterisk labels indicate statistical significance of the non-treated and mAb-treated groups compared to the LPS-stimulated group unless otherwise specified. ns $p > 0.05$, *$p < 0.05$, **$p < 0.01$, ***$p < 0.001$, ****$p < 0.0001$.

adhered monocytes upon the endothelialized hydrogel surface (Fig. 6c–e, i–k) from transmigrated monocytes deeper within the hydrogel matrix (Fig. 6f–h, l–n) using a combination of bright-field microscopy and Giemsa staining. After imaging, preliminary cell counts were conducted to observe how LPS stimulation and anti-VCAM-1 mAb treatment affected the proportion of monocytes that had adhered and transmigrated per unit area of the gel constructs. Contrary to the previous adhesion models, the number of adhered monocytes on the gel surface was significantly lower ($P < .05$) for the LPS-stimulated group compared to all other test groups (Fig. 6a). However, the number of transmigrated monocytes in LPS-stimulated group was significantly higher than the non-treated and mAb-treated groups (Fig. 6b).

Importantly, all antibody-treated groups exhibited monocyte adhesion levels comparable to the baseline (unstimulated) condition, indicating that the anti-VCAM-1 antibodies effectively blocked VCAM-1 availability in LPS-stimulated cells. Moreover, these antibodies significantly reduced monocyte transmigration compared to both LPS-stimulated and unstimulated conditions, further highlighting their excellent performance. The low number of adhered monocytes in the LPS-stimulated group can be attributed to their rapid transmigration into the hydrogel construct. When examining the two graphs together, the data does indeed suggest that the LPS-stimulated group exhibited a higher degree of transmigration compared to the other test groups, resulting in a significantly lower proportion of monocytes remaining adhered to the endothelial surface. Overall, the trend

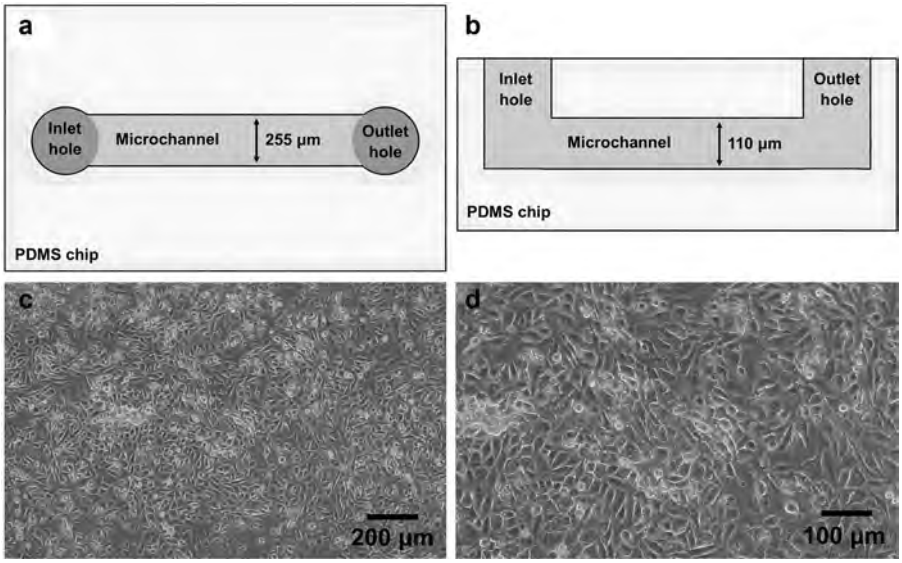

Figure 3. The microfluidics-based endothelial microvessel model used for the flow adhesion assay. (a-b) Schematic diagram of the single-channel microfluidics chip illustrated from the (a) top and (b) side view. The channel dimensions are 255 μm × 110 μm (W × H). (C-D) Brightfield microscopy images were taken at (c) 10× and (d) 20× magnification to confirm the successful formation of an endothelial monolayer over the microchannel surface. All representative images have been taken from a series of 3 independent experiments (N = 3).

observed with the antibody-treated groups would suggest that VCAM-1 treatment effectively inhibited both the monocyte adhesion and transmigration steps of the recruitment cascade.

As the results obtained from microscopy analysis only accounted for the number of cells per unit area of the 3D cell constructs, we performed a second quantification procedure to calculate the number of non-adhered, adhered, and transmigrated monocytes throughout the entire matrix volume. This method allowed us to account for possible heterogeneity of cell distribution throughout the hydrogel constructs and common visual interpretation biases from microscopy imaging [31]. After initiating the cell transmigration assay as described above, monocytes were collected and counted in the three stages of recruitment– non-adhesion, adhesion, and transmigration – using a conventional Giemsa smear method. Firstly, non-adhered monocytes were retrieved from the media supernatant left after incubating cell-hydrogel constructs with monocyte suspension for 1 h (Fig. 7b). Secondly, adhered monocytes were obtained after an additional 24 h incubation period by trypsinizing and resuspending the endothelial monolayer seeded atop the hydrogel surface (Fig. 7c). Finally, the transmigrated monocytes inside the gel matrix were recovered by collagenase digestion of the remaining hydrogel constructs (Fig. 7c). The selective nature of Giemsa staining for leukocytes allowed these cells to be easily distinguished from the other endothelial and smooth muscle cells in the complete co-culture [24].

After the first monocyte treatment period (Fig. 7b), the static transmigration assay could be used to indirectly determine the effects of VCAM-1 impact on monocyte adhesion by quantifying the number of non-adhered monocytes. As expected, LPS stimulation increased initial monocyte adhesion to endothelial monolayers (Fig. 7d), as demonstrated by a significantly lower number ($P < .01$) of non-adhered cells free floating in the supernatant compared to the non-treated endothelium. Furthermore, anti-VCAM-1 mAb treatment effectively reversed this effect, with all four mAbs exhibiting significantly higher ($P < .05$) numbers of non-adhered cells compared to the LPS-stimulated group. Then, after the second monocyte incubation period (Fig. 7c), the proportion of adhered and transmigrated monocytes was quantified. Much like in the preliminary cell count of monocyte adhesion (Fig. 7a) calculated from the brightfield microscopy method, Fig. 7e shows that the number of monocytes adhering to the endothelium after 24 h was significantly lower ($P < .05$) for the LPS-stimulated group compared to the non-treated and antibody treated groups. Even more, the number of transmigrated monocytes was significantly higher ($P < .01$) for the LPS-stimulated group compared to the other test groups (Fig. 7f). Taken together, the results show that the positive control mAb and the three mAb candidates were successful in blocking monocyte transmigration—with the number of transmigrated monocytes decreasing by 89.2% after treatment with the 429 mAb, 89.5% with 2E2 mAb, 84.6% with 3C12 mAb, and 82.3% with 3H4 mAb (Fig. 7e, f). Importantly, the cumulative results of the non-adhered, adhered, and transmigrated cell counts show that our VCAM-1 mAbs effectively inhibited monocyte recruitment at two separate steps of the cascade– cell adhesion and cell transmigration.

Discussion

The pathophysiological role of VCAM-1 in atherosclerosis has been well documented [32]. This association has seen VCAM-1 utilized as a targeting moiety in several antibody- and peptide-conjugated drug delivery systems for site-specific visualization and treatment of atherosclerotic lesions [9]. However, research into the therapeutic mechanisms of anti-VCAM-1 antibodies outside of these targeting abilities remains strikingly limited [8]. In addition to mediating leukocyte-endothelial adhesion and trafficking, VCAM-1 regulates endothelial signalling pathways related to oxidative stress and vascular permeability [33]. Considering this, researchers may be able to precisely modulate the anti-inflammatory activities of VCAM-1-targeted therapeutics by designing peptides and antibody antagonists that target specific domains of the VCAM-1 protein. In previous experiments, Perera *et al.* [11] generated a panel of novel scFvs against VCAM-1 using phage display biopanning technology, which appear to bind different domains of VCAM-1, and which were subsequently

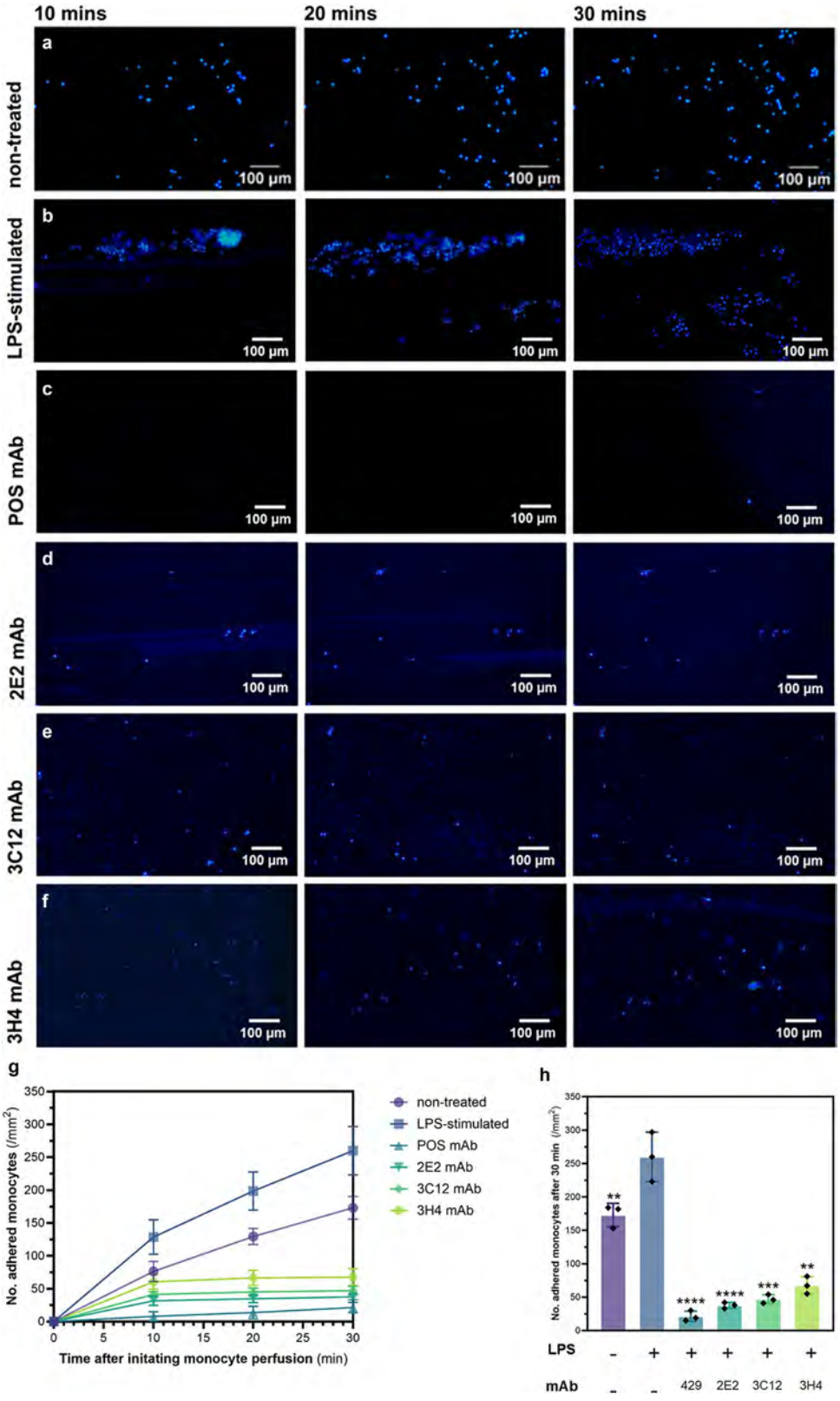

Figure 4. Testing the ability of novel anti-VCAM-1 mAb candidates to inhibit monocyte adhesion under flow using the endothelium-on-the-chip model. Hoechst-labelled RAW264.7s were perfused through LPS-stimulated and anti-VCAM-1 mAb-treated SVEC4-10 microvessels seeded within single-channel microfluidics chips. (a-f) Representative fluorescent images of monocyte adhesion to endothelial microvessels taken at 10, 20, and 30 min after initiating monocyte perfusion following (a) no treatment, (b) LPS stimulation, or LPS stimulation followed by treatment with (c) positive control anti-VCAM-1 429 mAb, (d) 2E2 mAb, (e) 3C12 mAb, and (f) 3H4 mAb. (g) Cell adhesion was quantified at each time point by automatically counting labelled monocytes in 4 random fields of view observed at 20× magnification (0.5 mm2). (h) Group comparison of control and treatment groups at the 30-min time point. Graphs show the mean +/- SD of 3 independent experiments (N = 3) experiments with one replica per experiment analyzed by ANOVA and post-hoc Tukey testing. Asterisk labels indicate statistical significance of the non-treated and mAb-treated groups compared to the LPS-stimulated group unless otherwise specified. ns $p > 0.05$, *$p < 0.05$, **$p < 0.01$, ***$p < 0.001$, ****$p < 0.0001$.

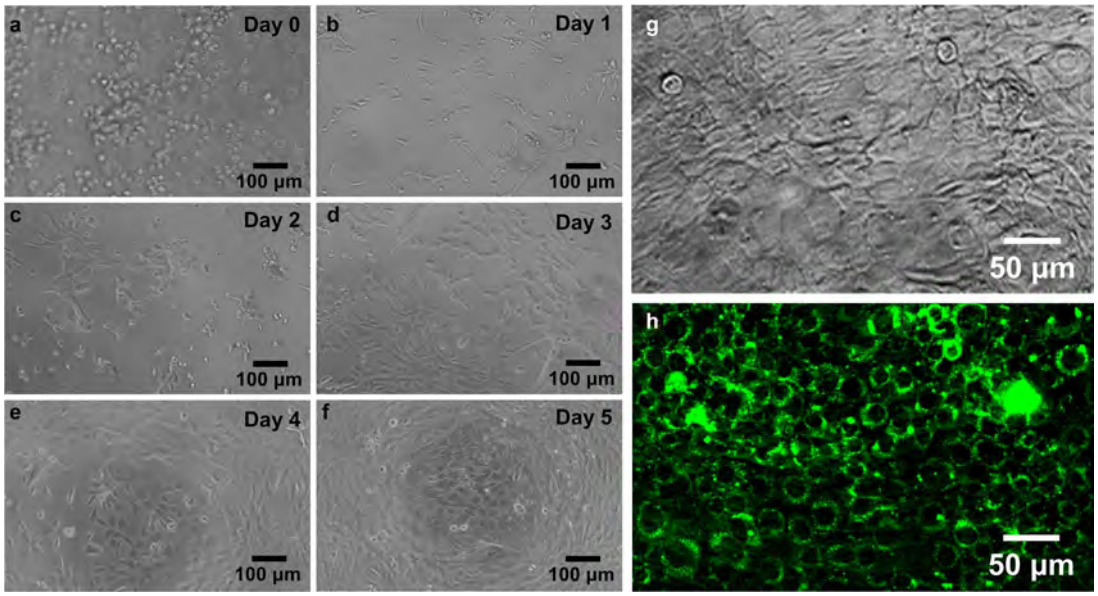

Figure 5. Establishing a confluent endothelial monolayer on top of the cell-hydrogel constructs. (a-f) Brightfield microscopy was taken at 20× magnification each day after seeding and before refreshing media to monitor endothelial cell growth and spreading on the hydrogel surface. VE-cadherin immunostaining was performed once cells reached confluency to visually confirm endothelial cell contact integrity. Representative (g) brightfield and (h) fluorescence microscopy images at 40× magnification show homogenous distribution of fluorescently labelled VE-cadherin, indicating that adherens junctions had been well-established between confluent endothelial cells. Shown are representative images of 4 independent experiments, with one replica per experiment (N = 4).

reformatted into mAbs to be tested in this study. Through a series of competitive binding (Fig. 2 and Fig. 4) and migration (Fig. 6 and Fig. 7) assays representing vascular inflammation *in vitro*, we were able to evaluate the therapeutic potential of our mAb candidates for atherosclerosis. The initial static adhesion assay depicted in Fig. 2 demonstrated that all candidates of the mAb panel were able to significantly reduce ($P < .05$) monocyte attachment to LPS-stimulated endothelial monolayers—with 2D8, 3H4, 3C12, and 2E2 mAbs being the most effective (listed in order of least to greatest impact on binding). Our results using mouse anti-VCAM-1 antibodies to block murine monocyte adhesion to murine endothelial are similar to Park *et al.*'s [10] human anti-VCAM-1 mAbs in a human cell adhesion assay. Together, these results demonstrate that binding to monocytes' Fc receptors does not prevent the antibodies' ability to significantly reduce cell adhesion, a result directly relevant to future clinical applications.

Several endothelial ligands—each exhibiting overlapping and complementary involvement in cell recruitment—could be considered drug targets for atherosclerosis therapy. The inducible nature of VCAM-1 means that it is selectively upregulated at sites of vascular dysfunction, marking it as an especially attractive target for precise and localized therapeutic activity [34]. As selectively inhibiting one specific vascular receptor leaves the opportunity for compensation by other related ligands, choosing a drug target that is functionally involved in all the stages of the transendothelial migration cascade is essential. The interaction between VCAM-1 on activated vascular endothelial cells and α_4 integrin on circulating monocytes is critical in mediating the transition from weak leukocyte rolling and adhesion to firm arrest and transmigration [8, 35]. The standard microplate (Fig. 2) and microfluidics-based (Fig. 4) adhesion assays employed in this study demonstrated that our mAb candidates were able to inhibit both weak monocyte-endothelial adhesions in a static environment and stronger adhesive interactions under flow. Furthermore, we were able to show that the mAbs were able to inhibit both adhesion and transmigration by employing the 3D hydrogel model (Fig. 6 and Fig. 7) despite the possibility of compensation by other endothelial receptors. Dose-response studies were not conducted as part of this study, though future investigations of multiple treatment concentrations would greatly improve comparisons on the potential therapeutic efficacy of the mAb candidate panel.

VCAM-1 is predominantly expressed in humans as a seven-domain protein in which the first, second, and third domains are highly homologous to the fourth, fifth, and sixth domains, respectively [36]. Domains 1 and 4 have both been implicated in monocyte attachment due to the presence of integrin-binding isoleucine-aspartate-serine-proline-leucine (IDSPL) amino acid sequence motifs recognized by complementary $\alpha_4\beta_1$ and $\alpha_4\beta_7$ integrins [37]. Naturally, these two domains are considered target epitopes for anti-VCAM-1 antibodies to block pathological cell recruitment during inflammatory disease. However, a few studies have developed antibodies to domains other than 1 and 4, suggesting the possibility of interfering with VCAM-1 function via these non-$\alpha_4\beta_1$ and $\alpha_4\beta_7$ integrin binding domains [10, 12, 38]. The positive control 429 antibody used in this study inhibits domains 1 and 2 [11]. Of the four most effective mAb candidates tested in this study, 2D8 and 2E2 have both previously demonstrated binding to domain 3 of murine VCAM-1 [11], whereas 3H4 binds to domain 2 [11], and 3C12 binds to domain 1 (data not shown in Perera *et al.* [11]). The ability of 3C12 to inhibit monocyte recruitment can likely be attributed to the competitive blockade of the α_4 integrin-binding sequence in domain 1 [37]. While the possible mechanisms of the other three mAbs have not been clearly linked to blocking the specific functions of domain 2 or 3, steric hindrance is a likely explanation for their adhesion-blocking effects. The presence of domain 2 has been previously identified as a structural requirement for the binding function of domain

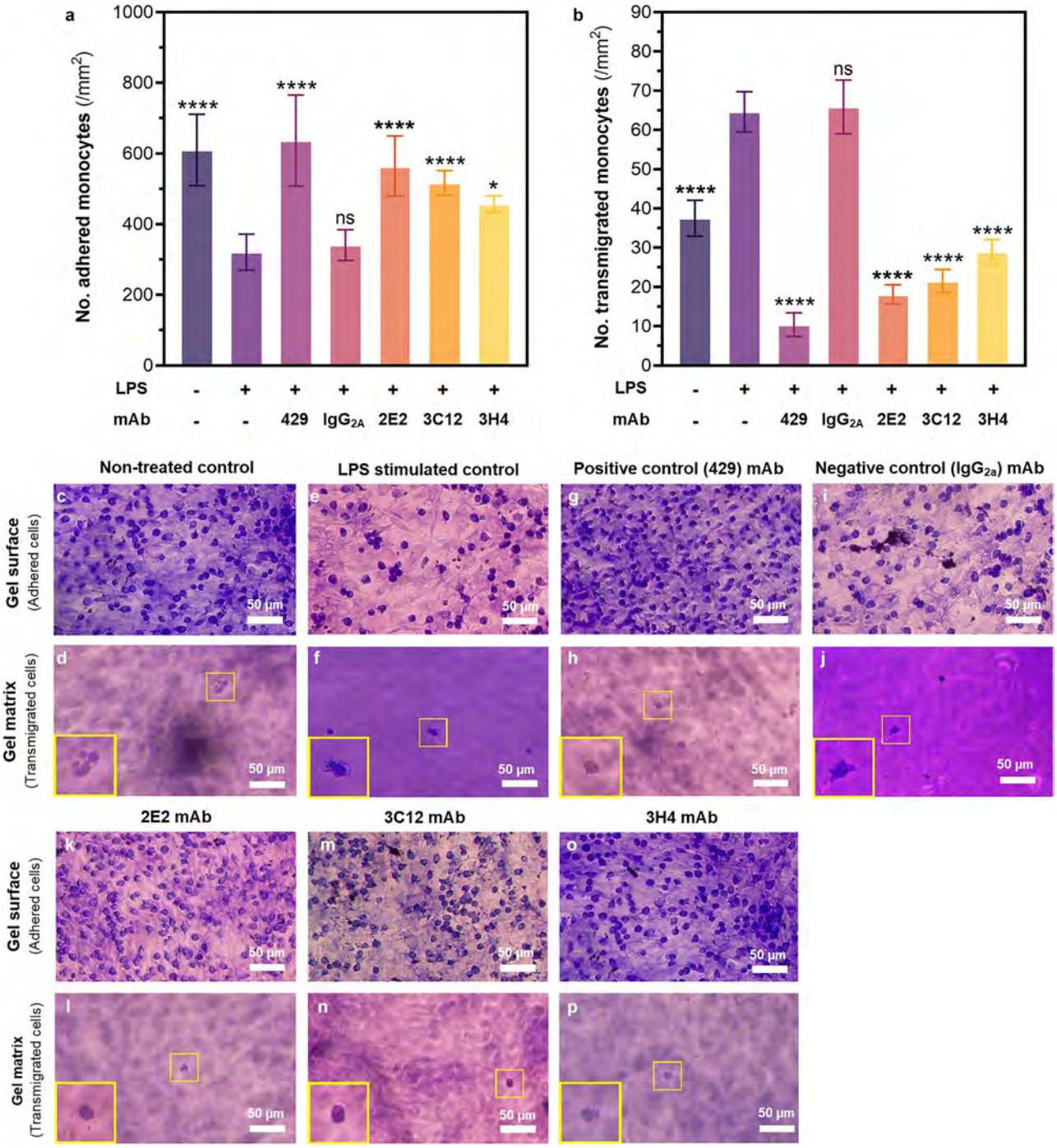

Figure 6. Visualizing monocyte adhesion and transmigration within the cell-hydrogel constructs using Giemsa staining and brightfield microscopy. Endothelialized cell-hydrogel constructs were incubated with monocytes to observe cell attachment and migration, then fixed and stained for visualization. Preliminary cell counts of (a) cell adhesion and (b) transmigration per unit area (/mm2) of hydrogel were performed for group comparison. Representative brightfield microscopy images were taken at 20× magnification to visualize adhered cell on the endothelialized hydrogel surface and within the gel matrix (c-d) non-treated, (e-f) LPS-stimulated, (g-h) anti-VCAM-1 429 mAb-treated, (i-j) negative isotype control-treated, (k-l) 2E2 mAb-treated, (m-n) 3C12 mAb-treated, and (o-p) 3H4 mAb-treated cell-hydrogel models. Stained monocytes were counted from 4 random fields of view observed at 20× magnification (0.5 mm2). Yellow boxes depict close-up images of individual monocytes at 40× magnification. Graphs show the mean +/- SD of 4 independent experiments with 2 technical replicates (total N = 8) analyzed by ANOVA and post-hoc Tukey testing. Asterisk labels indicate statistical significance of the non-treated and mAb-treated groups compared to the LPS-stimulated group unless otherwise specified. ns $p > 0.05$, *$p < 0.05$, **$p < 0.01$, ***$p < 0.001$, ****$p < 0.0001$.

1, whereas the role of domain 3 in VCAM-1 function is yet to be elucidated [39].

Considering the novelty of selectively targeting domain 2 or 3 of VCAM-1 as a strategy for directly combating monocyte recruitment, the tested mAbs represent an intriguing platform for site-specific atherosclerosis nanotherapeutics. The H6 and 7H mAbs previously tested with *in vitro* and *in vivo* models of atherosclerosis by Park *et al.* [10] bound within domains 1 or 2

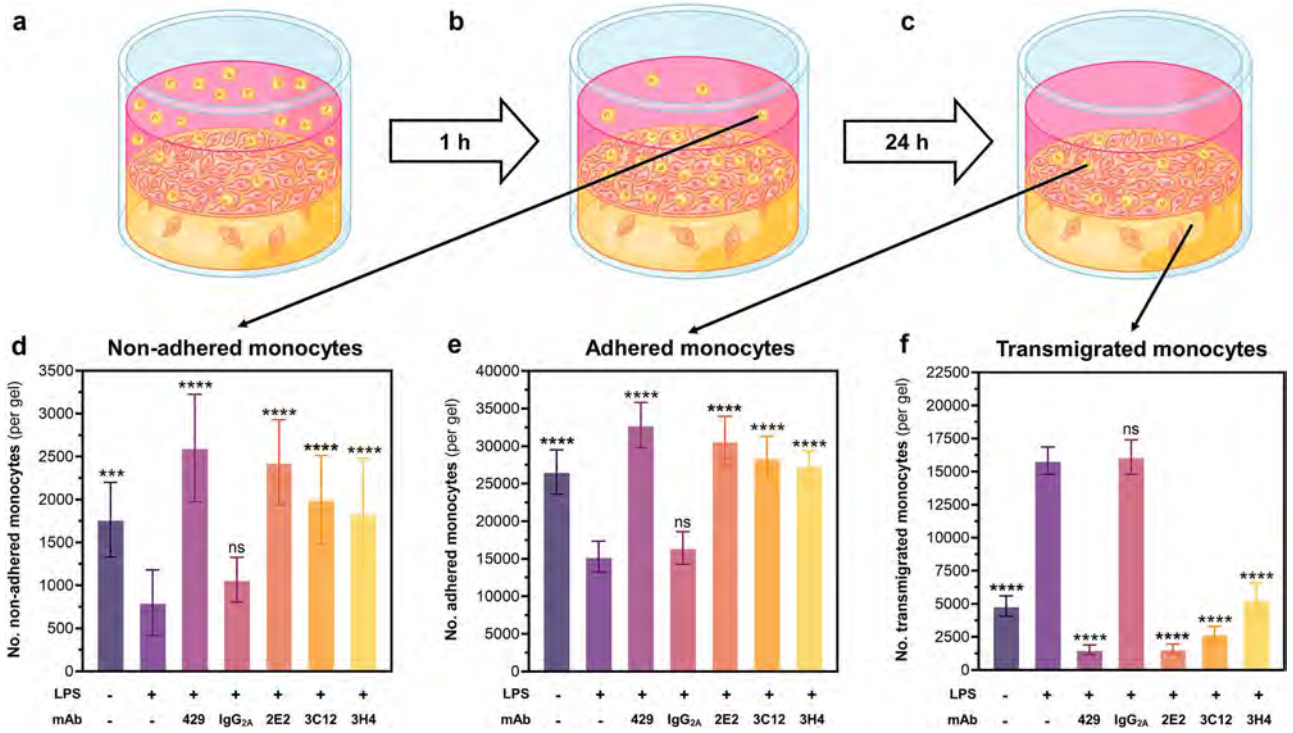

Figure 7. Comparing monocyte adhesion and transmigration of monocytes in LPS-stimulated endothelialized 3D collagen constructs with novel anti-VCAM-1 mAb treatments. As described in the experimental section, (a) monocytes were added onto the cell-hydrogel constructs and left for 1 h to allow adhesion. (b) After this time point, non-adhered monocytes in the supernatant were collected and the constructs were left to incubate for a further 24 h. (c) After this incubation period, adhered and transmigrated monocytes were separated and quantified by subsequent trypsinization and collagen gel digestion. (d) Non-adhered cells were collected by rinsing cell-hydrogel constructs with DPBS, pooling the supernatants, and counting cells using the haemocytometer. (e) Adhered cells were quantified by detaching the endothelial monolayer with trypsin, selectively Giemsa staining monocytes, and counting using a Giemsa smear with brightfield microscope. (f) Transmigrated cells were collected by digesting the cell-hydrogel constructs in collagenase, selectively staining monocytes with Giemsa, and counting all stained cells within a Giemsa smear. Graphs show the mean +/- SD of 4 independent experiments with 3 sample replicates each (total N = 12) analyzed by ANOVA and post-hoc Tukey testing. Asterisk labels indicate statistical significance of the non-treated and mAb-treated groups compared to the LPS-stimulated group unless otherwise specified. ns $p > 0.05$, *$p < 0.05$, **$p < 0.01$, ***$p < 0.001$, ****$p < 0.0001$.

of VCAM-1. The data presented in our study, however, shows that an anti-VCAM-1 mAb specific to domain 2 and not domain 1– 3H4 mAb –was able to reduce monocyte adhesion (Fig. 2 and Fig. 4) and transmigration (Fig. 6 and Fig. 7) using *in vitro* models of early atherosclerosis. There are also instances in the literature of mAbs against domain 3 of VCAM-1– which is the domain targeted by our 2E2 mAb –demonstrating inhibitory activity against inflammation-induced monocyte recruitment [40–42]. A possible explanation for the effectiveness of the 3H4 and 2E2 mAbs is that the domains they target may possess functional involvement in endothelial signalling pathways necessary for monocyte adhesion and migration. However, this hypothesis would warrant further investigation to determine the effects of our antibody candidates on signal transduction and protein expression. For example, the VCAM-1 protein activates several pathways involved in the clathrin-dependent internalization of VE-cadherin at endothelial cell-to-cell junctions, resulting in increased paracellular permeability during vascular inflammation [8, 33, 43]. The ability of our antibodies to inhibit monocyte transmigration *in vitro* could be interpreted as a preliminary indicator of interference with this pathway, though further study would be necessary to verify this. Of course, steric hindrance is another possibility for the efficacy of the anti-VCAM-1 mAbs, in which the antibodies physically block interactions between VCAM-1 and their complementary ligands. With this in mind, the mechanistic implications and potential synergy of combining treatment with mAbs that target different domains of the VCAM-1 protein is an interesting avenue for future studies with these antibody candidates.

As an important note, VCAM-1 is one of several types of adhesive surface receptors expressed on the activated endothelium during vascular inflammation – including E-selectin, P-selectin, and intracellular adhesion molecule (ICAM). While selectins mediate low-affinity interactions involved in monocyte rolling on the endothelium, VCAM-1 can facilitate firmer, more stable, cell attachments required for transendothelial migration due to its high-affinity binding to $\alpha_4\beta_1$ integrin on activated monocytes [44]. The ICAM-1 receptor, however, demonstrates high affinity binding to β_2 integrins on circulating monocytes and can support firm cell attachment and transmigration in a manner similar to that of VCAM-1 [27]. It is therefore important to acknowledge that antibody suppression of VCAM-1 is theoretically unable to completely ablate monocyte transmigration due to compensation by ICAM-1 and, though to a lesser extent, E- and P-selectin. The effect is this receptor compensation is evident from the residual levels of monocyte attachment and transmigration after anti-VCAM-1 mAb treatment observed across all assays employed in this study. Nonetheless, VCAM-1 blockade with therapeutic antibodies can still be considered a viable strategy for inhibiting monocyte recruitment associated with vascular disease progression, especially because VCAM-1 expression is present in 82% of atherosclerotic lesions compared to only 46% for ICAM-1 [45].

The microfluidic and 3D *in vitro* models employed in this study represent novel and sophisticated pre-clinical testing platforms compared to conventional cell culture assays due to their abilities to replicate certain physiological parameters of the human vascular system. For the microfluidic model, the peristaltic flow rate (31 μl/min) perfused through the device had been calculated to match the physiological shear stress (1000 s^{-1}) observed in human arteries [19]. Then for the 3D model, the composition of the hydrogel matrix incorporated collagen and smooth muscle cells to simulate the extracellular environment of the subendothelial space within human blood vessels [21]. However, it is also important to acknowledge the limitations of using murine cell lines for modelling human disease processes, especially in terms of clinical translation. In the context of this study, our findings still hold physiological relevance due to the structural and functional similarities between the human and mouse variants of the VCAM-1 protein. All known human and murine isoforms of VCAM-1 contain specific binding sites for the $\alpha_4\beta_1$ integrin ligand, though with varying degrees of binding affinity [46]. Therefore, the anti-VCAM-1 mAbs in our study could reasonably be predicted to inhibit VCAM-1 activity in human tissues based on the effects on cell adhesion we observed using murine endothelial cells. Nonetheless, it would improve the clinical relevance of these *in vitro* models to modify the designs to incorporate human cell lines as a future research direction.

In conclusion, this study demonstrates the therapeutic potential of a novel panel of anti-VCAM-1 mAbs for treating atherosclerosis by employing a series of *in vitro* models mimicking vascular inflammation. Our results show that all seven antibody candidates were able to effectively inhibit monocyte adhesion under static conditions. Furthermore, the three most effective mAbs– 2E2, 3C12, and 3H4 –were able to inhibit cell adhesion in a flow-based microfluidic model and cell transmigration in a 3D hydrogel construct model. The novelty of these antibody candidates—particularly regarding their binding activity to VCAM-1 domains other than domains 1 and 4—highlights the importance of antibody discovery technology for discovering and identifying new molecular mechanisms for combatting multifactorial disease pathologies such as atherosclerosis.

Author contributions

Jessica R. Pickett (Formal Analysis [lead], Investigation [lead], Methodology [equal], Visualization [lead], Writing—original draft [lead]), Lucia F. Zacchi (Conceptualization [supporting], Investigation [supporting], Methodology [supporting], Resources [equal], Writing—review & editing [equal]), Binura Perera (Investigation [supporting]), Yuao Wu (Investigation [supporting], Methodology [supporting], Supervision [supporting], Writing—review & editing [supporting]), and Hang Ta (Conceptualization [lead], Funding acquisition [lead], Methodology [lead], Project administration [lead], Resources [lead], Supervision [lead], Writing—review & editing [equal])

Supplementary data

Supplementary data are available at *ABT* online.

Conflict of interest

The authors declare no conflict of interests.

Funding

This work was supported by the National Health and Medical Research Council (APP1182347, and APP2002827 to H.T.T.), National Heart Foundation of Australia (102761 to H.T.T.), and a Promoting Women Fellowship from the University of Queensland to L.F.Z. J.P is supported by a Griffith University PhD scholarship. Elements of this research utilized the facilities and resources of the National Biologics Facility (NBF), and Australian National Fabrication Facilities (ANFF), University of Queensland. NBF is supported by Therapeutic Innovation Australia (TIA). TIA is supported by the Australian Government through the National Collaborative Research Infrastructure Strategy (NCRIS) program.

Data availability

Data will be made available upon request.

Ethics and consent statement

Not applicable.

Animal research statement

Not applicable.

References

1. Jebari-Benslaiman, S, Galicia-García, U, Larrea-Sebal, A *et al.* Pathophysiology of atherosclerosis. *Int J Mol Sci* 2022; **23**: 3346. https://doi.org/10.3390/ijms23063346.
2. Morrison, AM, Sullivan, AE, Aday, AW. Atherosclerotic disease: Pathogenesis and approaches to management. *Med Clin North Am* 2023; **107**: 793–805. https://doi.org/10.1016/j.mcna.2023.04.004.
3. Libby, P. The changing landscape of atherosclerosis. *Nature* 2021; **592**: 524–33. https://doi.org/10.1038/s41586-021-03392-8.
4. Libby, P, Everett, BM. Novel Antiatherosclerotic therapies. *Arterioscler Thromb Vasc Biol* 2019; **39**: 538–45. https://doi.org/10.1161/ATVBAHA.118.310958.
5. Cinoku, II, Mavragani, CP, Moutsopoulos, HM. Atherosclerosis: Beyond the lipid storage hypothesis. The role of autoimmunity. *Eur J Clin Invest* 2020; **50**: e13195. https://doi.org/10.1111/eci.13195.
6. Solanki, A, Bhatt, LK, Johnston, TP. Evolving targets for the treatment of atherosclerosis. *Pharmacol Ther* 2018; **187**: 1–12. https://doi.org/10.1016/j.pharmthera.2018.02.002.
7. Yin, M, Li, C, jiang, J *et al.* Cell adhesion molecule-mediated therapeutic strategies in atherosclerosis: From a biological basis and molecular mechanism to drug delivery nanosystems. *Biochem Pharmacol* 2021; **186**: 114471. https://doi.org/10.1016/j.bcp.2021.114471.
8. Pickett, JR, Wu, Y, Zacchi, LF *et al. Targeting endothelial vascular cell adhesion molecule-1 in atherosclerosis: Drug discovery and development of vascular cell adhesion molecule-1-directed novel therapeutics* Cardiovasc. *Res.* 2023; **119**: 2278–93. https://doi.org/10.1093/cvr/cvad130.
9. Castro, R, Adair, JH, Mastro, AM *et al.* VCAM-1-targeted nanoparticles to diagnose, monitor and treat atherosclerosis. *Nanomedicine (Lond)* 2024; **19**: 723–35. https://doi.org/10.2217/nnm-2023-0282.
10. Park, J-G, Ryu, SY, Jung, IH *et al.* Evaluation of VCAM-1 antibodies as therapeutic agent for atherosclerosis in apolipoprotein

E-deficient mice. *Atherosclerosis* 2013; **226**: 356–63. https://doi.org/10.1016/j.atherosclerosis.2012.11.029.
11. Perera, B, Wu, Y, Pickett, JR *et al.* Isolation and characterization of antibodies against VCAM-1 reveals putative role for Ig-like 2 and 3 domains in cell-to-cell interaction. *Int J Mol Sci* 2024; **25**: 13650. https://doi.org/10.3390/ijms252413650.
12. Lee, S, Yoon, IH, Yoon, A *et al.* An antibody to the sixth Ig-like domain of VCAM-1 inhibits leukocyte Transendothelial migration without affecting adhesion. *J Immunol* 2012; **189**: 4592–601. https://doi.org/10.4049/jimmunol.1103803.
13. Chen, J, Zhang, X, Millican, R *et al.* Recent progress in in vitro models for atherosclerosis studies. *Front Cardiovasc Med* 2022; **8**: 790529. https://doi.org/10.3389/fcvm.2021.790529.
14. Panagides, N, Zacchi, LF, de Souza, MJ *et al.* Evaluation of phage display biopanning strategies for the selection of anti-cell surface receptor antibodies. *Int J Mol Sci* 2022; **23**: 8470. https://doi.org/10.3390/ijms23158470.
15. Schindelin, J, Arganda-Carreras, I, Frise, E *et al.* Fiji: An open-source platform for biological-image analysis. *Nat Methods* 2012; **9**: 676–82. https://doi.org/10.1038/nmeth.2019.
16. McDonald, JC, Duffy, DC, Anderson, JR *et al.* Fabrication of microfluidic systems in poly(dimethylsiloxane). *Electrophoresis* 2000; **21**: 27–40. https://doi.org/10.1002/(SICI)1522-2683(20000101)21:1<27::AID-ELPS27>3.0.CO;2-C.
17. Akther, F, Sajin, S, Moonshi, S *et al.* An intimal-lumen model in a microfluidic device: potential platform for atherosclerosis-related studies. *Lab Chip* 2025; **25**: 354–69. https://doi.org/10.1039/D4LC00868E.
18. Akther, F, Yakob, SB, Nguyen, NT *et al.* Surface modification techniques for endothelial cell seeding in PDMS microfluidic devices. *Biosensors (Basel)* 2020; **10**: 182. https://doi.org/10.3390/bios10110182.
19. Akther, F, Zhang, J, Tran, HDN *et al.* Atherothrombosis-on-Chip: A site-specific microfluidic model for thrombus formation and drug discovery. *Adv Biol* 2022; **6**: e2101316. https://doi.org/10.1002/adbi.202101316.
20. Akther, F, Little, P, Li, Z *et al.* Hydrogels as artificial matrices for cell seeding in microfluidic devices. *RSC Adv* 2020; **10**: 43682–703. https://doi.org/10.1039/D0RA08566A.
21. Akther, F, Sajin, D, Moonshi, SS *et al.* Modeling foam cell formation in a hydrogel-based 3D-intimal model: A study of the role of multi-diseases during early atherosclerosis. *Adv Biol (Weinh)* 2024; **8**: e2300463. https://doi.org/10.1002/adbi.202300463.
22. Beaudry, KL, Parsons, CLM, Ellis, SE *et al.* Localization and quantitation of macrophages, mast cells, and eosinophils in the developing bovine mammary gland. *J Dairy Sci* 2016; **99**: 796–804. https://doi.org/10.3168/jds.2015-9972.
23. Kobayashi, S, Saio, M, Fujimori, M *et al.* Macrophages in Giemsa-stained cerebrospinal fluid specimens predict carcinomatous meningitis. *Oncol Lett* 2020; **20**: 352. https://doi.org/10.3892/ol.2020.12217.
24. Angelovich, TA, Hearps, AC, Maisa, A *et al.* Quantification of monocyte transmigration and foam cell formation from individuals with chronic inflammatory conditions. *J Vis Exp* 2017; **128**: 56293. https://doi.org/10.3791/56293.
25. Dauphinee, SM, Karsan, A. Lipopolysaccharide signaling in endothelial cells. *Lab Invest* 2006; **86**: 9–22. https://doi.org/10.1038/labinvest.3700366.
26. Bradfield, PF, Johnson-Léger, CA, Zimmerli, C *et al.* LPS differentially regulates adhesion and transendothelial migration of human monocytes under static and flow conditions. *Int Immunol* 2007; **20**: 247–57.
27. Walpola, PL, Gotlieb, AI, Cybulsky, MI *et al.* Expression of ICAM-1 and VCAM-1 and monocyte adherence in arteries exposed to altered shear stress. *Arterioscler Thromb Vasc Biol* 1995; **15**: 2–10. https://doi.org/10.1161/01.ATV.15.1.2.
28. Mohan, S, Mohan, N, Valente, AJ *et al.* Regulation of low shear flow-induced HAEC VCAM-1 expression and monocyte adhesion. *Am J Physiol* 1999; **276**: C1100–7. https://doi.org/10.1152/ajpcell.1999.276.5.C1100.
29. Ramos, CL, Huo, Y, Jung, U *et al.* Direct demonstration of P-selectin- and VCAM-1-dependent mononuclear cell rolling in early atherosclerotic lesions of apolipoprotein E-deficient mice. *Circ Res* 1999; **84**: 1237–44. https://doi.org/10.1161/01.RES.84.11.1237.
30. Huo, Y, Hafezi-Moghadam, A, Ley, K. Role of vascular cell adhesion Molecule-1 and fibronectin connecting Segment-1 in monocyte rolling and adhesion on early atherosclerotic lesions. *Circ Res* 2000; **87**: 153–9. https://doi.org/10.1161/01.RES.87.2.153.
31. Lee, RM, Eisenman, LR, Khuon, S *et al.* Believing is seeing—the deceptive influence of bias in quantitative microscopy. *J Cell Sci* 2024; **137**: jcs261567. https://doi.org/10.1242/jcs.261567.
32. Ley, K, Huo, Y. VCAM-1 is critical in atherosclerosis. *J Clin Invest* 2001; **107**: 1209–10. https://doi.org/10.1172/JCI13005.
33. Cook-Mills, JM, Marchese, ME, Abdala-Valencia, H. Vascular cell adhesion Molecule-1 expression and Signaling during disease: Regulation by reactive oxygen species and antioxidants. *Antioxid Redox Signal* 2011; **15**: 1607–38. https://doi.org/10.1089/ars.2010.3522.
34. Nakashima, Y, Raines, EW, Plump, AS *et al.* Upregulation of VCAM-1 and ICAM-1 at atherosclerosis-prone sites on the endothelium in the ApoE-deficient mouse. *Arterioscler Thromb Vasc Biol* 1998; **18**: 842–51. https://doi.org/10.1161/01.ATV.18.5.842.
35. Weber, C, Springer, TA. Interaction of very late antigen-4 with VCAM-1 supports transendothelial chemotaxis of monocytes by facilitating lateral migration. *J Immunol* 1998; **161**: 6825–34. https://doi.org/10.4049/jimmunol.161.12.6825.
36. Imhof, BA, Dunon, D. Leukocyte migration and adhesion. *Adv Immunol* 1995; **58**: 435–16.
37. Chuluyan, HE, Osborn, L, Lobb, R *et al.* Domains 1 and 4 of vascular cell adhesion molecule-1 (CD106) both support very late activation antigen-4 (CD49d/CD29)-dependent monocyte transendothelial migration. *J Immunol* 1995; **155**: 3135–4. https://doi.org/10.4049/jimmunol.155.6.3135.
38. Lee, J-H, Sohn, JH, Ryu, SY *et al.* A novel human anti-VCAM-1 monoclonal antibody ameliorates airway inflammation and remodelling. *J Cell Mol Med* 2013; **17**: 1271–81. https://doi.org/10.1111/jcmm.12102.
39. Renz, ME, Chiu, HH, Jones, S *et al.* Structural requirements for adhesion of soluble recombinant murine vascular cell adhesion molecule-1 to alpha 4 beta 1. *J Cell Biol* 1994; **125**: 1395–406. https://doi.org/10.1083/jcb.125.6.1395.
40. Graber, N, Gopal, TV, Wilson, D *et al.* T cells bind to cytokine-activated endothelial cells via a novel, inducible sialoglycoprotein and endothelial leukocyte adhesion molecule-1. *J Immunol* 1990; **145**: 819–30. https://doi.org/10.4049/jimmunol.145.3.819.
41. Bochner, BS, Luscinskas, FW, Gimbrone, MA Jr *et al.* Adhesion of human basophils, eosinophils, and neutrophils to interleukin 1-activated human vascular endothelial cells: Contributions of endothelial cell adhesion molecules. *J Exp Med* 1991; **173**: 1553–7. https://doi.org/10.1084/jem.173.6.1553.
42. Damle, NK, Aruffo, A. Vascular cell adhesion molecule 1 induces T-cell antigen receptor-dependent activation of CD4+T

lymphocytes. *Proc Natl Acad Sci U S A* 1991; **88**: 6403–7. https://doi.org/10.1073/pnas.88.15.6403.
43. Abdala-Valencia, H, Cook-Mills, JM. VCAM-1 signals activate endothelial cell protein kinase cα via oxidation. *J Immunol* 2009; **177**: 6379–87.
44. Gerhardt, T, Ley, K. Monocyte trafficking across the vessel wall. *Cardiovasc Res* 2015; **107**: 321–30. https://doi.org/10.1093/cvr/cvv147.
45. Singh, V, Kaur, R, Kumari, P *et al.* ICAM-1 and VCAM-1: Gatekeepers in various inflammatory and cardiovascular disorders. *Clin Chim Acta* 2023; **548**: 117487. https://doi.org/10.1016/j.cca.2023.117487.
46. Troncoso, MF, Ortiz-Quintero, J, Garrido-Moreno, V *et al.* VCAM-1 as a predictor biomarker in cardiovascular disease. *Biochim Biophys Acta Mol Basis Dis* 2021; **1867**: 166170. https://doi.org/10.1016/j.bbadis.2021.166170.

Antibody Therapeutics, 2025, 8(4), 350–363
https://doi.org/10.1093/abt/tbaf025
Research Article

Supporting Information for

Assessing the therapeutic potential of a panel of novel VCAM-1 antibodies using microfluidic and three-dimensional *in vitro* models of vascular inflammation

Materials & Method

Materials

All chemicals were reagent-grade and did not require further purification unless specified otherwise. SYLGARD™ 184 Silicone Elastomer Kit (1317318) was purchased from Dow Corning. Cultrex® 3-D Culture Matrix Rat Collagen I (3447-020-01) was purchased from In Vitro Technologies. Collagen solution from bovine skin (C4243), collagenase D from *Clostridium histolyticum* (11088858001), 3,3-dihexyloxacarbocyanine iodide ($DiOC_6$, 318426) Dulbecco's Modified Eagle Medium (DMEM, D5796), ethanol, Giemsa stain (G4507), isopropyl alcohol, lipopolysaccharide (LPS) from *Escherichia coli* (L2143), methanol, paraformaldehyde (PFA, 16005), and sodium hydroxide were purchased from Sigma-Aldrich. Bovine serum albumin (BSA, A8531), Dulbecco's phosphate-buffered saline (DPBS, D8537), foetal bovine serum (10099141), Hoechst 33342 staining solution (62249), penicillin-streptomycin (P/S, 15140122), 2.5% (w/v) trypsin (15090046), and TrypLE™ Express enzyme (12604021) were purchased from Thermo Fisher Scientific.

Regarding the control and test antibodies, goat anti-rabbit IgG H&L (Alexa Fluor® 488) mAb (Abcam #ab150077, RRID: AB_2630356) and rabbit anti-mouse recombinant anti-VCAM-1 (EPR5047) mAb (Abcam #ab134047, RRID: AB_2721053) were purchased from Abcam. Rat anti-mouse anti-VCAM-1 (CD106) 429 mAb (Thermo Fisher Scientific #14-1061-82, RRID: AB_467419), rat anti-mouse VE-cadherin (CD144, Alexa Fluor® 488) BV13 mAb (Thermo Fisher Scientific #53-1441-80, RRID: AB_1210528), and mouse IgG isotype control (ThermoFisher Scientific #02-6502, RRID: AB_2532951) were purchased from Thermo Fisher Scientific.

Cell culture

SVEC4-10 (ATCC CRL-2181) endothelial cells, RAW264.7 (ATCC TIB-71) macrophage, and MOVAS (ATCC CRL-2797) smooth muscle cell lines were obtained from the American Type Culture Collection (ATCC). RAW264.7 macrophages were maintained in complete, low-glucose (1 mg/mL) DMEM supplemented with 10% FBS and 1% P/S. SVEC4-10 and MOVAS cells were maintained in complete, low-glucose DMEM supplemented with 10% FBS and 1% P/S. All cell culture vessels were stored at 37 °C in a humidified incubator at 5% CO_2 atmosphere and passaged following manufacturer guidelines using TrypLE™ Express cell dissociation reagent.

Static monocyte adhesion assay on the microplate

The static monocyte-endothelial cell adhesion assay we employed for competitive binding inhibition studies of the antibody panel was optimized based on a previous adhesion assay protocol described by Park *et al*.[10] SVEC cells (passages 8-10) were plated on a 96-well microtitre plate at a density of 2.0×10^4 cells per well and cultured in DMEM for 24 h at 37 °C. All subsequent treatment steps were performed by introducing 100 µL reagent solution to each well after rinsing with DPBS unless specified otherwise. The seeded SVEC cells were stimulated with 100 ng/mL LPS for 24 h at 37 °C and then pre-treated with 20 µg/mL anti-VCAM-1 mAbs (positive control 429 mAb, IgG isotype negative control mAb, and anti-VCAM-1 1A9, 2D3, 2D8, 2E2, 2E6, 3C12, 3H4 IgG_{2a} clones) for 1 h at 37 °C. Concurrently, RAW macrophages (passages 15-17) were fluorescently labelled by incubating with 50 ng/mL $DiOC_6$-supplemented DMEM and then centrifuge-washed (700 × *g*, 5 min, 20 °C) to remove excess stain. The $DiOC_6$-labelled macrophages were added to the plated cell monolayers at a density of 1.0×10^4 cells per well and incubated in the dark at 37 °C for 10 min to allow cell attachment. After incubating, all wells were washed twice with DPBS to remove unbound macrophages and fixed with 4% (w/v) PFA at room temperature for 20 min.

Fluorescence spectrophotometry and microscopy of static binding assay

Fluorescence analysis of the static monocyte adhesion assay was performed using two separate quantitative methods: plate reader spectrophotometry and fluorescence microscopy. The cumulative fluorescence of the adherent $DiOC_6$-labelled macrophages in each well was measured using a BMG LABTECH CLARIOstar® microplate reader with excitation set to 480 nm and emission set to 520 nm. Samples were blank-corrected against 100 µL DPBS and normalized to the non-antibody-treated, LPS-stimulated control wells for group comparison. Fluorescence microscopy images were captured using the OLYMPUS CKX53 fluorescence

microscope with a Cool LED pE-300 light source, OLYMPUS-DP74 camera, and Olympus cellSens™ imaging software. Cell adhesion was quantified from fluorescent microscopy images using Fiji (Version v1.54k for Windows, University of Wisconsin, United States) image processing software.[14] Labelled monocytes within 3 randomly selected fields at 20× magnification (0.5mm^2/field) were automatically counted within each well, and then the mean number of adherent cells per mm^2 was calculated.

Microfluidics chip fabrication

Microfluidics chips were fabricated according to standard photolithography and polydimethylsiloxane (PDMS) soft lithography techniques.[18] PDMS pre-polymer was mixed with SYLGARD™ 184 Silicone Elastomer at a 10:1 mass ratio to create a solid elastomer with optimum biocompatibility for cell culture. The PDMS mixture was degassed in a desiccator for 5-10 min, poured onto a silicon master mould corresponding to the appropriate channel design, and then cured at 75 °C for 2 h to allow the PDMS to solidify. Once the PDMS slabs were separated from the master mould, the edges were cut, and then inlet and outlet holes were punched with a 1 mm-diameter needle. The slabs were then washed with 70% (v/v) isopropyl alcohol and distilled water and then dried at 75 °C for 5 min. Finally, the PDMS chip was tightly sealed to a clean glass slide by treating it with oxygen plasma for 1.5 min using a Harrick Plasma PDC-32G Plasma Cleaner. For this study, the design of the microfluidic device consisted of a single rectangular microchannel chamber (255 µm wide and 100 µm high) with circular inlet and outlet ports (100 µm in diameter).

Microvessel formation in the microfluidics device

Endothelial cells were seeded within the microfluidic devices using a protocol previously reported by Akther *et al.*[19] After chip fabrication and bonding, the microfluidic device was sterilized by exposing it to ultraviolet light for 1 h, perfusing the microchannel with 70% (v/v) ethanol for 10 min, and then washing twice with DPBS. The inner surface of the microchannel was then functionalized with 0.4 mg/mL bovine skin collagen solution to counter the inherent hydrophobicity of PDMS for optimal endothelial cell adhesion to the PDMS substrate.[20] For cell seeding, a 1.5×10^7 cells/mL suspension of SVEC cells (passage <10) was injected through the inlet port of the microchannel by manual pipetting. The chip was then incubated at physiological temperature with orbital shaking (200 rpm) for 1 h to expose the system to oscillatory flow during the period of initial cell-substrate attachment. Afterwards, the device was incubated at 37 °C and 5% CO_2 for an additional 4 h, flipping the chip at the halfway time

point to support the formation of a complete 3D microvessel covering all faces of the rectangular microchannel.[19]

Before commencing with the flow-based cell adhesion assay, the seeded SVEC cells were cultured in the microchannel under controlled flow conditions to allow the formation of a uniform endothelial microvessel. The microfluidic device was attached to a peristaltic pump (NE-9000 PeriPumpONE New Era Pump Systems) via the inlet and outlet ports of the microchannel to subject the microvessel to continuous peristaltic flow. All components of the peristaltic circuit were connected using silicon tubing (1.5 mm diameter), which had been sterilized beforehand with 70% (v/v) ethanol for 30 min and ultraviolet light for 1 h. Once attached to the pump circuit, the microfluidic device was maintained at 37 °C and 5% CO_2 until required for microscopy. For the first 12 h of incubation, the pump was initially set to a low flow rate (12 µL/min) to avoid disrupting cell-substrate attachment and proliferation while still exposing the cell monolayer to moderate shear stress. The flow rate was then increased to representative blood flow rate (31 µL/min) for a further 24 h to allow sufficient time for the seeded cell monolayer to form a uniform endothelial microvessel. This flow rate was calculated to equate to typical arterial shear rate (1000 s^{-1}) based on the dimensions of the microchannel and Newton's Law of Viscosity.[21] All subsequent treatments introduced into the microfluidic device were perfused at this flow rate unless specified otherwise.

Flow-based monocyte adhesion assay on the microfluidic chip

Once a confluent monolayer covering all faces of the rectangular microchannel had been established, the microvessel was stimulated by perfusing 1 µg/mL LPS-supplemented DMEM through the microfluidic circuit for 8 h. Using the same perfusion technique, devices were subjected to anti-VCAM-1 mAb (429 positive control mAb, and 2E2, 3C12, 3H4 IgG_{2a} clones) pre-treatment for 2 h before commencing with the flow adhesion assay. For this step, RAW macrophages were fluorescently labelled with Hoechst stain (1 µg/mL, 30 min, 30 °C) and injected through the microchannel using a syringe pump (NE-1000 Master Dual Syringe Pump, New Era Pump Systems) to observe real-time monocyte rolling and adhesion under continuous flow. Fluorescence microscopy images were taken at three 10-min intervals after initiating monocyte perfusion into the microchannel. Cell adhesion was quantified from microscopy images using an automatic cell counter in Fiji. Using a similar approach to that described in **Section 2.5**, the number of adherent cells per mm^2 was calculated by automatically counting Hoechst-labelled monocytes within 3 randomly selected fields on the microchannel surface at 20× magnification (0.5 mm^2/field).

Formation of cell-hydrogel constructs for three-dimensional cell culture

Cell-hydrogel constructs were prepared from Cultrex® Rat Collagen I and MOVAS smooth muscle cells (passage <10) according to the manufacturer's protocol. In summary, 2 mg/mL collagen and 1.0×10^5 cells/mL MOVAS cells were suspended in high-glucose (5 mg/mL) DMEM and neutralized to pH 7 with 1M NaOH (e.g. add 8 µL of 1M NaOH to 500 µL of hydrogel). The collagen and smooth muscle cell components of the resultant hydrogel matrices served to model the extracellular microenvironment of the vascular subendothelial space.[22] For our 3D transmigration experiments, 50 µL gel precursor mixture per well was added to a tissue culture-treated 96-well microtitre plate and incubated (37 °C, 5% CO_2) for 1 h to allow the gels to set. After gel solidification was confirmed, hydrogel constructs were endothelialized with an SVEC cell monolayer using a protocol previously reported by Akther *et al.*[23] Briefly, 100 µL of 2.0×10^5 cells/mL SVEC suspension in high-glucose DMEM was added to each gel-coated well and cultured for 5 days to allow a confluent endothelial monolayer to form. Media was refreshed every 24 h to maintain the overall viability of the cell-hydrogel constructs and endothelial monolayers.

Endothelial barrier integrity of the confluent monolayers was confirmed using a standard VE-cadherin immunostaining procedure based on previous methods obtained from the literature.[24, 25] Endothelialized cell-hydrogel constructs were prepared as described in Section 2.6.1 to facilitate the formation of a confluent EC monolayer on the hydrogel surface. For all steps of immunostaining, 100 µL of reagent solution was introduced and incubated at RT unless specified otherwise. The cell-hydrogel constructs were fixed with 4% PFA for 1 h, rinsed once with DPBS, blocked with 1% BSA, and then rinsed again with DPBS. The cells were then labelled by incubating with eBioScience™ CD144 mAb (diluted in 1:100 in DPBS) at 4°C O/N. Once immunostaining was completed, the constructs were rinsed 3 times with DPBS before performing brightfield and fluorescent microscopy imaging for qualitative analysis of endothelial barrier integrity.

Monocyte transmigration assay under static, non-flow conditions

Once the endothelial monolayers were grown to confluency upon the hydrogel, the cells were incubated (37 °C, 5% CO_2) with 100 ng/mL LPS for 24 h to stimulate endothelial activation during vascular disease. Cell-hydrogel constructs were then pre-treated with 20 µg/mL anti-VCAM-1 mAbs (429 positive control, and 2E2, 3C12, 3H4 IgG_{2a} clones) and incubated for 1 h. After rinsing the constructs once with DPBS, 2.0×10^4 RAW macrophages were added to each well and incubated for 1 h to allow enough time for initial monocyte-endothelial

attachment while ensuring enough cells remained in the supernatant for meaningful comparison between treatment groups. To collect the non-adhered cells for counting, the gel constructs were rinsed twice with 100 μL of DPBS, then the pooled supernatants and rinse solutions (300 μL total) from each well were aliquoted. The total number of non-adhered cells from each well was calculated using a conventional haemocytometer counting method. The monocyte-treated constructs were then replenished with fresh DMEM and incubated for an additional 24 h to ensure measurable levels of cell migration occurred before commencing with further analysis.

Visual assessment of monocyte transmigration by Giemsa stain microscopy

To qualitatively assess the effects of inflammatory stimulation and antibody pre-treatment on monocyte transmigration across endothelial monolayers, we treated the cell-hydrogel constructs with Giemsa stain and performed brightfield microscopy analysis. Giemsa stain selectively stains leukocytes, allowing macrophages to be effectively differentiated from endothelial and smooth muscle cells in the hydrogel matrix.[26, 27] Before commencing Giemsa staining, hydrogel constructs were fixed with 4% PFA at room temperature for 1 h. All steps were performed by incubating cell-hydrogel constructs with 100 μL reagent solution at room temperature unless specified otherwise. The protocol was as follows: the cells were fixed with 50% (v/v) methanol for 5 min, 78% (v/v) methanol for 15 min, stained with 5% (w/v) Giemsa working solution (diluted in 1:3:16 glycerine-to-methanol-to-water) for 20 min, then washed thoroughly with water to remove excess stain. For brightfield microscopy, gels were removed from the 96-well plate and placed onto a glass coverslip face down so that the endothelial monolayer was in contact with the glass surface. Brightfield focus was initially adjusted so that the endothelial monolayer was in the field of view, then shifted into the hydrogel matrix to count the total number of transmigrated monocytes. As a preliminary cell counting technique, adhered monocytes on the endothelial monolayer and transmigrated monocytes in the gel matrix were quantified per unit area from a randomly selected field of view for each gel using a similar method to that previously employed for the static adhesion assay.

Quantitative measurement of transmigration by Giemsa smear

After qualitative microscopy analysis, an adapted Giemsa smear method was employed to quantitatively compare the inhibitory effects of our anti-VCAM-1 mAb candidates on monocyte adhesion and transmigration under static conditions. Cell-hydrogel constructs were fabricated, and the monocyte transmigration assay was performed as described in **Sections 2.10** and **2.11**. Non-transmigrated monocytes on the hydrogel surface were collected by incubating

the cell-hydrogel constructs with 100 µL of 2.5% (w/v) trypsin at room temperature and washing thoroughly with an equivalent volume of DPBS until the endothelial monolayer had been entirely detached. The supernatant and rinse solutions were then pooled (200 µL total) for each gel, centrifuged at 300 × *g* for 5 min, and aliquoted for Giemsa smearing and cell counting. Monocytes were selectively stained for counting using a modified Giemsa smear protocol adapted from the literature.[28] Briefly, a 10 µL suspension of the adherent monocytes and endothelial cells detached from the hydrogel substrate after trypsinization was smeared onto a clean glass cover slip. The cover slip was dipped in 100% (v/v) methanol for cell fixation, air-dried for 30 s, and then stained with Giemsa working solution at room temperature for 30 min before rinsing with deionized water. All Giemsa-stained monocytes within the smear were visualized and counted under a brightfield microscope, and the total number of adhered monocytes per gel was calculated.

To collect transmigrated cells encapsulated within the gel matrix, the trypsinized hydrogels were digested in 100 µL of 0.25% (w/v) collagenase D in DPBS and incubated at 37 °C for 10-15 min until disaggregation was observed. As with the rinse solutions, the liquified gels were collected, centrifuged, resuspended, and stored on ice until ready for the Giemsa staining procedure. Transmigrated monocytes were stained for cell counting and analysis using the same Giemsa smear method described above.

Statistical analysis

All data was expressed as mean ± standard deviation of the mean (SDM) and annotated with degrees of significance (*$p < 0.05$, **$p < 0.01$, ***$p < 0.005$, ****$p < 0.001$). The total number of experimental replicates (N), which includes both independent experiments and sample replicates, are indicated in the figure legends for each experiment. The mean differences of monocyte adhesion and transmigration between antibody-treated groups and controls were analysed using one-way analysis of variance (ANOVA) followed by post-hoc Tukey for pairwise comparisons. Values of $p < 0.05$ were considered statistically significant. All data visualization and statistical analyses were conducted with GraphPad Prism 10 (Version 10.3.1 for Windows, GraphPad Software, San Diego, United States).

Results

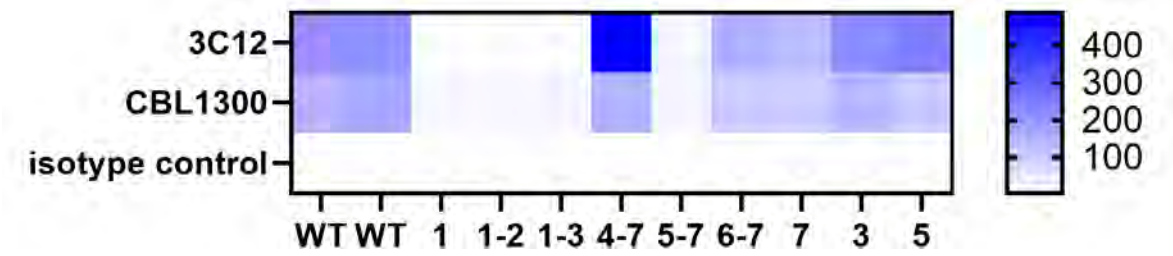

Supplementary Figure S1: Clone 3C12 binds Ig-like domain 1 of mVCAM-1. The 3C12 clone was developed by Perera *et al.* and tested simultaneously with the other clones described in that manuscript (please refer to Figure 4, Results, and Methods in Perera *et al.*). Binding of the 3C12 clone to different domains of VCAM-1 was assessed by flow cytometry, using Ig-like domain deletion versions of VCAM-1 C-terminally tagged with GFP and N-terminally tagged with FLAG (to show extracellular expression) transiently expressed in CHO cells. Cells were stained with commercial rat anti-mVCAM-1 antibody (Millipore, Burlington, MA, USA, Cat# CBL1300, RRID:AB_2214062) as positive control, $mIgG_{2a}$ isotype negative control (Miltenyi Biotec, Bergisch Gladbach, Germany, Cat# 130-106-546, RRID:AB_2661589), or clone 3C12 in $mIgG_{2a}$ format, followed by appropriate secondary antibodies. The table shows the normalized MFI (median fluorescence intensity) values for each of the antibody combinations, with lighter colors indicating lower antibody binding and darker colors indicating higher antibody binding. Displayed is the average normalized MFI (mVCAM-1-eGFP-positive+antibody-positive cells quadrant normalized to MFI of the mVCAM-1-eGFP-negative+antibody-positive cells quadrant) from one experiment with 2 replicates.

Supplementary Table S1: Summary of Tukey's multiple comparisons of non-treated and antibody-treated groups against the lipopolysaccharide (LPS)-stimulated group for spectrophotometric analysis of the static adhesion assay (**Figure 2M**).

Comparison	**Mean difference**	**95.00% CI of diff.**	**Significance**	**Adjusted P-value**
LPS-stimulated vs. **non-treated**	-37.04	-51.27 to -22.80	****	<0.0001
LPS-stimulated vs. **+VE** mAb	41.51	27.27 to 55.74	****	<0.0001
LPS-stimulated vs. **-VE** mAb	2.085	-12.15 to 16.32	ns	>0.9999
LPS-stimulated vs. **1A9** mAb	21.70	7.462 to 35.94	***	0.0002
LPS-stimulated vs. **2D3** mAb	16.63	2.396 to 30.87	*	0.0102

LPS-stimulated vs. **2D8** mAb	31.98	17.74 to 46.22	****	<0.0001
LPS-stimulated vs. **2E2** mAb	39.27	25.03 to 53.50	****	<0.0001
LPS-stimulated vs. **2E6** mAb	26.58	12.34 to 40.82	****	<0.0001
LPS-stimulated vs. **3C12** mAb	32.97	18.73 to 47.21	****	<0.0001
LPS-stimulated vs. **3H4** mAb	29.34	15.10 to 43.58	****	<0.0001

Supplementary Table S2: Summary of Tukey's multiple comparisons of non-treated and antibody-treated groups against the commercial-grade, anti-vascular cell adhesion molecule (VCAM-1) positive control antibody (429)-treated group for spectrophotometric analysis of the static adhesion assay (**Figure 2M**).

Comparison	**Mean difference**	**95.00% CI of diff.**	**Significance**	**Adjusted P-value**
+VE mAb vs. **non-treated**	4.470	-9.768 to 18.71	ns	0.9923
+VE mAb vs. **LPS-stimulated**	41.51	27.27 to 55.72	****	<0.0001
+VE mAb vs. **-VE** mAb	-39.42	-53.66 to -25.18	****	<0.0001
+VE mAb vs. **1A9** mAb	-19.81	-34.04 to -5.568	***	0.0009
+VE mAb vs. **2D3** mAb	-24.87	-39.11 to -10.63	****	<0.0001
+VE mAb vs. **2D8** mAb	-9.527	-23.77 to 4.711	ns	0.4835
+VE mAb vs. **2E2** mAb	-2.241	-16.48 to 12.00	ns	>0.9999
+VE mAb vs. **2E6** mAb	-14.93	-29.17 to -0.6904	*	0.0324
+VE mAb vs. **3C12** mAb	-8.537	-22.78 to 5.701	ns	0.6409
+VE mAb vs. **3H4** mAb	-12.17	-26.40 to 2.072	ns	0.1604